RSC Advances

ROYAL SOCIETY OF CHEMISTRY

www.rsc.org/advances

Thermoelectric Properties of Sol-gel Derived Lanthanum Titanate Ceramics

Xinrun Xiong, Ruoming Tian*, Xi Lin, Dewei Chu*, and Sean Li

Abstract

In this work, the thermoelectric properties of lanthanum titanate ceramics with different La/Ti ratios were reported. Samples were prepared using sol-gel method followed by conventional sintering process. At 973 K, the electrical resistivity of $La_{2/3}TiO_{2.87}$ ceramic is ~91 μΩm, with a Seebeck coefficient of -192 μV/K and the thermal conductivity is 2 W/m K. The ZT value of $La_{2/3}TiO_{2.87}$ is 0.18 at 973 K, demonstrating its potential for high temperature thermoelectric applications.

Introduction

Nowadays, thermoelectric materials have been widely explored to overcome the global warming and climate change issues by converting waste heat into electricity. A material governed by large Seebeck coefficient (S), high electrical conductivity (σ) and low thermal conductivity (k) is required for high ZT value [1]. Recently, perovskite-type oxides have been receiving great attention as thermoelectric materials because of their unique properties, e.g. non-toxicity and high temperature stability. For example, $SrTiO_3$ is a good candidate for n-type thermoelectric applications by appropriate substitutionally doping (La^{3+} and Nb^{5+}) [2, 3]. However, the ZT value of bulk $SrTiO_3$ has a large thermal conductivity of 4-12 W/K m ranging from room temperature to 1000 K of due to its simple cubic structure [4]. $CaMnO_3$, also considered as a high-temperature thermoelectric material, has been studied by doping rare earth elements at the Ca site with a ZT value closed to 0.3 at 1000 K [5, 6]. Despite the

School of Materials Science & Engineering, University of New South Wales Sydney NSW 2052 Australia
*Corresponding Author, Tel.: +61 (0)2 9385 5090; Fax: +61 (0)2 9385 6565
E-mail address: r.tian@unsw.edu.au, D.Chu@unsw.edu.au

aforementioned promising thermoelectric materials, lanthanum titanate is also an interesting perovskite oxide with tuneable phases [7]. It is well known as a standard band insulator due to the $3d^0$ configuration of Ti^{4+}. However, interesting electronic properties are expected for smaller valencies due to the non-empty Ti $3d^1$ orbital configuration [8]. In recent years, some studies have concentrated on electronic structure and transport properties of $La_{2/3+x}TiO_{3\pm\delta}$ [8-12]. By controlling the La/O stoichiometry, the electrical conductivity of lanthanum titanate can be enhanced by electron doping and the transition from insulating nature to metallic behavior can be easily achieved. The mechanism in this non-metal to metal transition can be ascribed to the oxygen defects in the crystalline structure, since it is well known that oxygen vacancy can generate two electrons and therefore contribute to the n-type conductivity [13-15].

Although there have been several studies on the electronic structure, electronic transport properties of $La_{2/3+x}TiO_{3\pm\delta}$, most of them are not related with thermal properties and there are hardly any reports in high temperature thermoelectric properties. In the present work, we reported high temperature thermoelectric properties of $La_{2/3}TiO_{2.87}$ ceramics. Sol-gel method has been selected to prepare ceramic powders due to its better control of stoichiometry and homogeneity compared to the conventional solid state method. By introducing La site vacancy and removing oxygen during the ceramic sintering procedure, $La_{2/3}TiO_{2.87}$ ceramic was prepared. The thermoelectric properties, i.e., electrical conductivity, Seebeck coefficient, thermal conductivity of $La_{2/3}TiO_{2.87}$ ceramics were measured and finally the dimensionless figure of merit was calculated from room to high temperature (373-973 K). The effect of the La/Ti ratio on the thermoelectric properties was also studied.

Experimental Section

Lanthanum titanate ceramics were prepared using a sol-gel process and conventional sintering method. Commercially available chemicals of Titanium (IV) bis(ammonium lactato) dihydroxide solution (TALH), Lanthanum(III) nitrate hexahydrate ($La(NO_3)_3{\cdot}6H_2O$), acetic acid (CH_3COOH) and 1, 2-propanediol ($CH_3CH(OH)CH_2OH$) were all purchased from Sigma-Aldrich without further

purification. In a typical synthesis, acetic acid was added to the TALH solution in a molar ratio of 1:10, to form the metal chelate followed by the addition of 1, 2-propanediol (acetic acid/1, 2-propanediol = 1:4, to promote the formation of polymer matrix). Then a certain amount of $La(NO_3)_3 \cdot 6H_2O$ was dissolved into DI water and mixed together with the above solution and stirred well at 353 K for 3h to obtain homogeneous sol. To promote esterification and polymerization process, the heating temperature was then increased to 393 K until gelation completed. Thereafter the yellow gel was aged 12 hours and heated in open air at 523 K for 2h yielding a brownish powder precursor. The powder precursor was then calcined in air at 1273 K for 2h to form lanthanum titanate powders.

The resultant lanthanum titanate powders, with different lanthanum/titanium ratios (La/Ti = 1 and La/Ti = 2/3) are notated as La-1 and La-2/3, respectively. The powder with different lanthanum ratios was pressed into a pellet with 20 mm in diameter and 2mm in thickness under a uniaxial pressure of 160 MPa. The pellet was then sintered at 1673 K for 6hrs in a reducing atmosphere with a mixture of 5% H_2/Ar.

In order to determine the calcination temperature, Simultaneous Thermal Analyzer (NETZSCH STA-449) was carried out. Differential Scanning Calorimeter (DSC) and thermogravimetric analysis (TGA) were used to identify the thermal transformations. The powder precursor was heated from room temperature up to 1273 K with a heating rate of 10 K/min in Air using Al_2O_3 crucibles**.** The Archimedes density measurement was used to determine the densities of as-prepared ceramics. XRD (Panalytical X'pert MPD) was used to identify the phase compositions of lanthanum titanate powders after calcination in air and the pellets after sintering in reducing gas. The microstructures of samples which were polished and thermally etched were analysed using a field-emission scanning electron microscope (NanoSEM 230). Carrier concentration and Hall mobility were determined using Hall measurement system (HL5500PC) for a square sample of about 10×10 mm^2 with a thickness of around 2 mm. The electrical conductivity and Seebeck coefficient were simultaneously measured using a ULVAC-ZEM3 system under the low-pressure helium atmosphere from room temperature to 1073K for a shaped-bar sample of about $3.5 \times 2 \times 10$ mm^3. The Thermal conductivity was obtained by separate measurements using DSC for heat capacity and laser flash system (NETZSCH LFA-427) for thermal diffusivity under the Ar atmosphere for a square sample of about 10×10 mm^2 with a thickness of

around 2 mm. The overall thermal conductivity was then evaluated from the thermal diffusivity (D), the heat capacity (C_p) and the experimental density (ρ) as a function of temperature (T), using the relationship: $k(T) = \alpha(T) \times C(T) \times \rho(T)$ [3].

Results and discussion

Thermogravimetric analyses (TGA) and differential scanning calorimetry (DSC) analyses were carried out to characterize the microstructural evolution of the gel to lanthanum titanate during the calcination process. Figure 1 shows the thermal behavior of the powder precursor with a heating rate of 10 K/min from 300 K to 1273 K. The TGA curve indicates a small weight loss up to 523 K, followed by a continuous weight loss region of ~25% in the temperature range of 523 K to 1023 K, and no further weight loss up to 1273 K. The first weight loss can be attributed to water desorption. The second abrupt weight loss region can be ascribed as the degradation of the organic components into CO_2 and H_2O. The DSC curve shows two exothermic peaks in the temperature range from 573 K to 873 K. These are associated with the weight loss shown in the TGA curve, which indicates the degradation of organic material from the gel. At higher temperature (~1023 K), the chemical reactions occurred and the lanthanum titanate phase began to form. Hence, the calcination temperature has to be higher than 1023 K, to obtain lanthanum titanate phase.

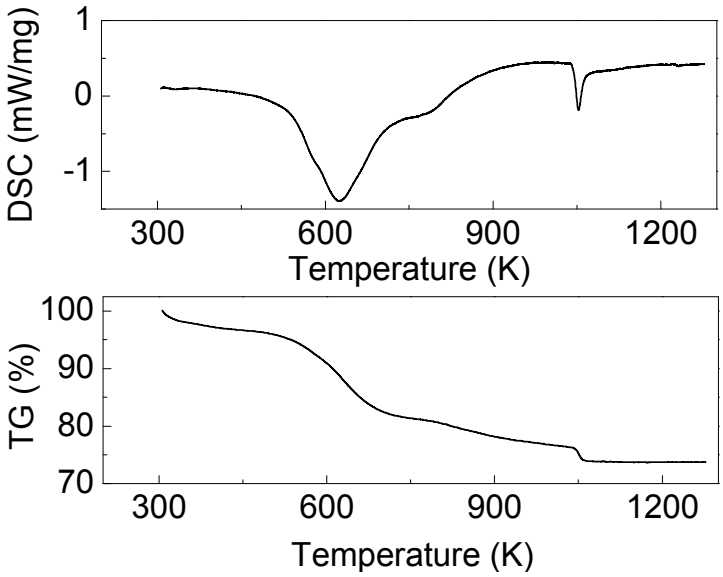

Figure 1 Thermal analysis of lanthanum titanate powder precursor using sol-gel method

The XRD patterns of calcinated powers with different La/Ti ratios (La-1 and La-2/3) are shown in **Figure 2**. Both powders were calcined at 1273 K for 2 hrs in open air. For La-1 powder, all the diffraction peaks can be identified as the $La_2Ti_2O_7$ phase with a space group of $P2_1$ by referring to the standard JCPD card (Ref 04-007-2817). However, different from the La-1 sample, the La-2/3 powder consists of two phases. One is the $La_2Ti_2O_7$ phase marked as the square symbols in Figure 2. The other is the $La_4Ti_9O_{24}$ phase (JCPD 04-013-3201) mainly due to the non-stoichiometry of La and Ti. According to these XRD results, the preferred phase for lanthanum titanate is $La_2Ti_2O_7$, which is reasonable since the most stable form of Ti ion in lanthanum titanate is tetravalent (4+) [8].

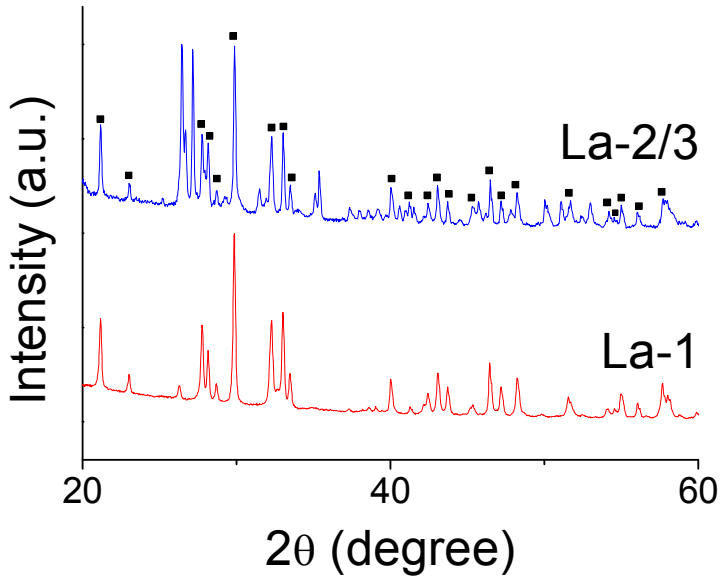

Figure 2 XRD patterns for lanthanum titanate powders with different lanthanum contents

The XRD patterns of the sintered pellets are shown in **Figure 3(a) and (b)**. The diffraction peaks of the La-1 sample are identified as the $La_2Ti_2O_7$ phase (JCPDS 04-007-2817), with some amount of $La_{2/3}TiO_{2.87}$, marked as the square symbols. The main peaks of as-prepared La-1 ceramic can be attributed to $La_2Ti_2O_7$ (JCPDS 04-007-2817). On the other hand, the existence of $La_{2/3}TiO_{2.87}$ phase (JCPDS 04-009-4053) can be attributed to the reducing condition during the sintering process. The removal of partial oxygen from the lanthanum titanate created a charge imbalance, and in order to neutralize additional positive charge, La vacancy emerged as a

consequence. Therefore, La-1 ceramic contains two different phases of $La_2Ti_2O_7$ and $La_{2/3}TiO_{2.87}$. The diffraction peaks of La-2/3 show a pure phase and can be indexed to the same standard $La_{2/3}TiO_{2.87}$ phase (JCPDS 04-009-4053). Also the SEM image of the as-prepared La-2/3 ceramic is shown in **Figure 3(c)**. The average grain size of the ceramic was estimated ranging from 5-20 μm. The relative densities of La-2/3 and La-1 pellets were found to be 87% and 96% respectively via the Archimedes density measurement.

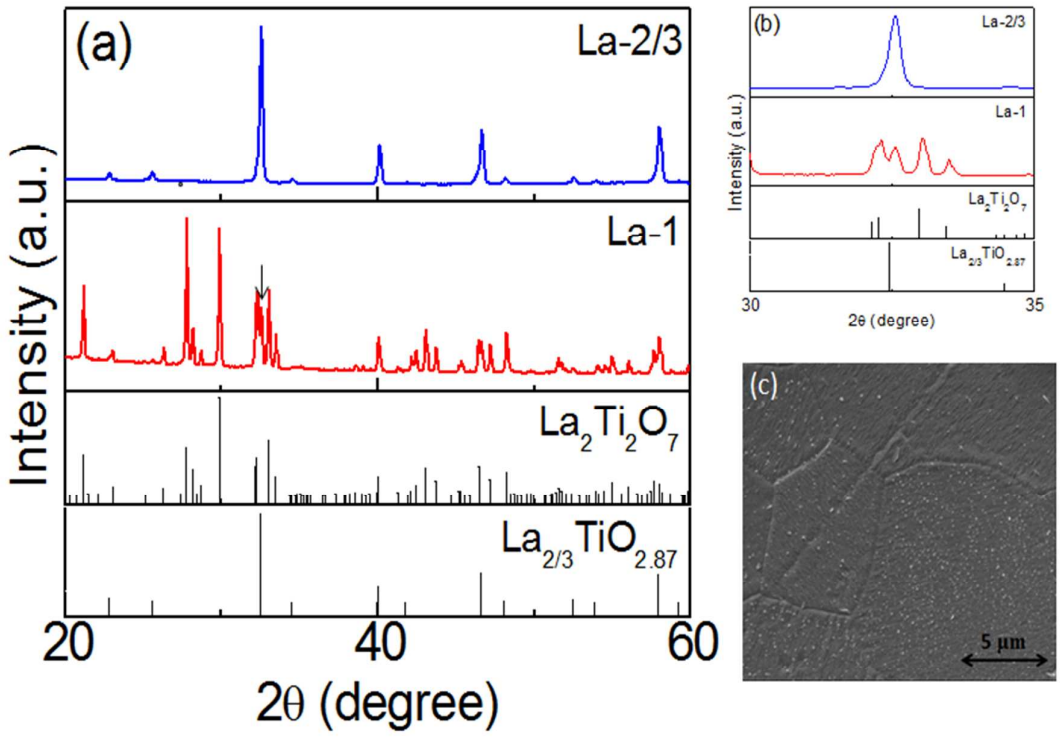

Figure 3 (a) XRD patterns for the sintered pellets with different La/Ti ratios (b) enlarged XRD patterns in the range of 30^0 and 35^0 for the sintered pellets with different La/Ti ratios (c) the SEM image of thermally-etched La-2/3 pellet.

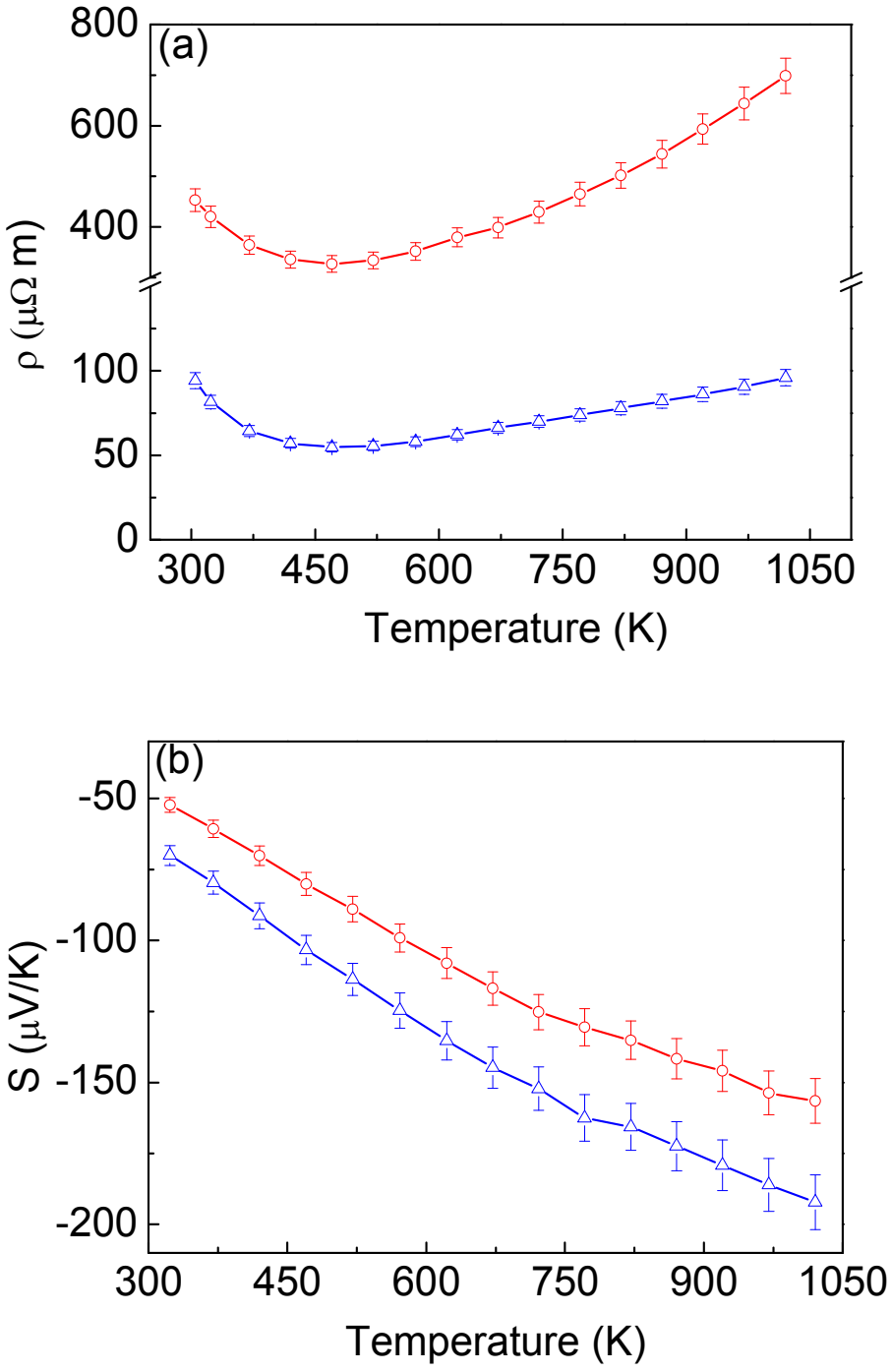

Figure 4 Electrical resistivity (ρ) and Seebeck coefficient (S) as a function of temperature: (Circle) La-1 (Triangle) La-2/3

Figure 4(a) shows the temperature dependence of electrical resistivity for lanthanum titanate-based ceramics. Both samples exhibited a semiconductor to metal transition around 450K, and the negative temperature coefficient of resistivity below 450K is

considered to be attributed to the small-polaron hopping mechanism, which is commonly found in other perovskite materials such as CaMnO3 [16] and BaTiO3 [17] . It clearly shows that La-2/3 ceramic possessed much lower resistivity of 100 μΩ m in the measured temperature range which is highly in agreement with Kim, et al. [10]. In their work, $La_{2/3}TiO_{2.852}$ ceramic had a resistivity of about 120 μΩ m and a Seebeck coefficient of around -40 μV/K at room temperature. Also there were some previous studies focused on the resistivity of lanthanum titanate thin film. Taguchi, et al. [8] and Gariglio, et al. [12] showed a resistivity of 30 μΩ m at room temperature which is slightly lower than that from our experimental results of 100 μΩ m. In comparison, the electrical resistivity of La-1 ceramic sample was more than four times higher than that of the La-deficient counterpart. It is reported that the resistivity of intrinsic $La_2Ti_2O_7$ phase is on the order of 10^{15} μΩ m at room temperature [18]. Therefore, the remarkable difference in the electrical resistivity values between the two samples is mainly attributed to the presence of $La_2Ti_2O_7$ phase.

Figure 4(b) shows the Seebeck coefficient (S) as a function of the temperature for both samples. The negative values of the Seebeck coefficient over the full range of temperature suggest that the dominant charge carriers in current system are electrons. Both samples exhibited an increasing trend of absolute values of Seebeck coefficient as the temperature increases. However, the La-2/3 possessed a higher Seebeck coefficient, which reached -192 μV/K at 1020 K. The difference in the Seebeck coefficient between the two samples is around 20 – 40 μV/K over all the temperature range. It is considered that such difference is possibly associated with the presence of $La_2Ti_2O_7$ phase and the grain boundaries between the two phases in the La-1 sample.

In order to further investigate the electronic transport mechanism inside these two samples, Hall Effect measurement was conducted at room temperature and the results are presented below in **Table 1**. It clearly shows that although the La-2/3 sample possessed a lower carrier concentration, its carrier mobility was one order of magnitude higher than that of the La-2/3 sample. According to the Mott Equation [19],

$$S = \frac{C_e}{n} + \frac{\pi^2 k_B^2 T}{3e}\left[\frac{\partial \ln \mu(\varepsilon)}{\partial \varepsilon}\right]_{\varepsilon=\varepsilon_F} \quad (2)$$

where $c_e = \left(\frac{\pi^2 k_B^2 T}{3e}\right)\psi(\varepsilon)$ and $n, \mu(\varepsilon), c_e, k_B,$ and $\psi(\varepsilon)$ are carrier concentration, energy correlated carrier mobility, specific heat, Boltzmann constant and density of state, respectively.

Therefore, a reduction in the carrier concentration and an increase in the mobility will lead to an increase in the Seebeck coefficient of La-2/3 sample, which is consistent with our measured result.

Table 1 Electrical resistivity (ρ), carrier concentration (n), Hall mobility (μ) and Seebeck coefficient (S) for La-1 and La-2/3 measured at room temperature

	ρ (μΩ m)	**n (cm^{-3})**	**μ ($cm^2 V^{-1} s^{-1}$)**	**S (μV K^{-1})**
La-1	453	-1.75×10^{20}	0.783	-47.6
La-2/3	68.3	-8.286×10^{19}	11.8	-61.8

Combining the electrical resistivity and the Seebeck coefficient, the power factors were calculated and shown in **Figure 5** as a function of temperature. It demonstrates that the power factor of the La-2/3 sample was more than one order of magnitude higher than that of the La-1sample, due to the simultaneous enhancement in electrical conductivity and Seebeck coefficient. For instance, it achieved ~ 4×10^{-4} W/mK^2 for the La-2/3 sample at 1020K. This power factor value is comparable to that of other thermoelectric materials, such as $CaMnO_3$ or $SrTiO_3$, which suggests that the as-synthesised La-2/3 ceramic sample can be potential thermoelectric candidate for high-temperature applications.

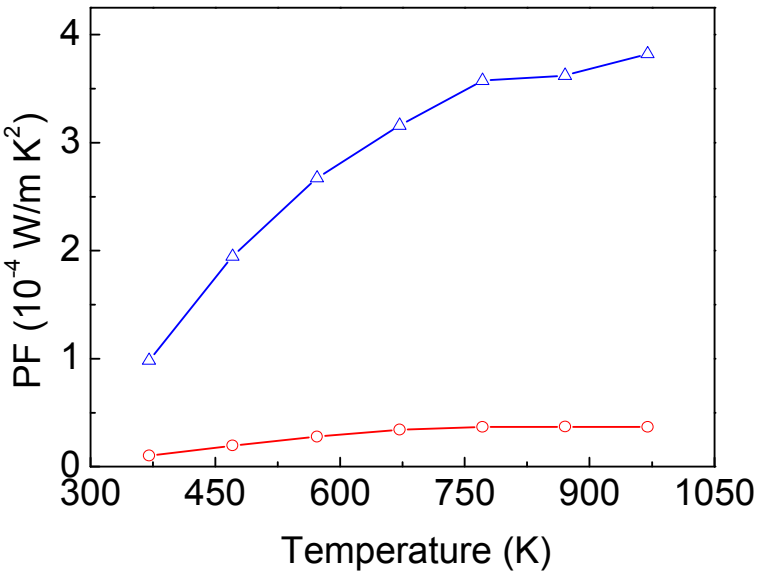

Figure 5 Temperature dependence of the power factor (PF): (Circle) La-1, (Triangle) La-2/3

The temperature dependence of the thermal conductivity (k) for both samples is depicted in **Figure 6**, which shows that thermal conductivity decreases with increasing temperature and the La-1 sample possessed lower thermal conductivity. The Wiedemann-Franz law has been employed here to estimate the contribution of electrons (k_{el}) and phonons ($k_{lattice}$) to the total thermal conductivity (k_{total}). The calculated electron thermal conductivity for both samples only accounted for 4~5 % of the total thermal conductivity. Therefore, the phonon term $k_{lattice}$ would dominate the thermal conductivity in both cases. The possible scenario for the lower thermal conductivity in La-1 sample is due to the presence of $La_2Ti_2O_7$ phase, which possesses a double perovskite structure and a low thermal conductivity (i.e., 0.37 W/m K at room temperature) [20]. Other factors may stem from the interfaces between the $La_2Ti_2O_7$ or $La_{2/3}TiO_{2.87}$ phases, which may help to scatter more phonons and to achieve a low thermal conductivity. However there was no previous study and supporting data available for the thermal properties of either $La_2Ti_2O_7$ or $La_{2/3}TiO_{2.87}$, further studies are under investigation.

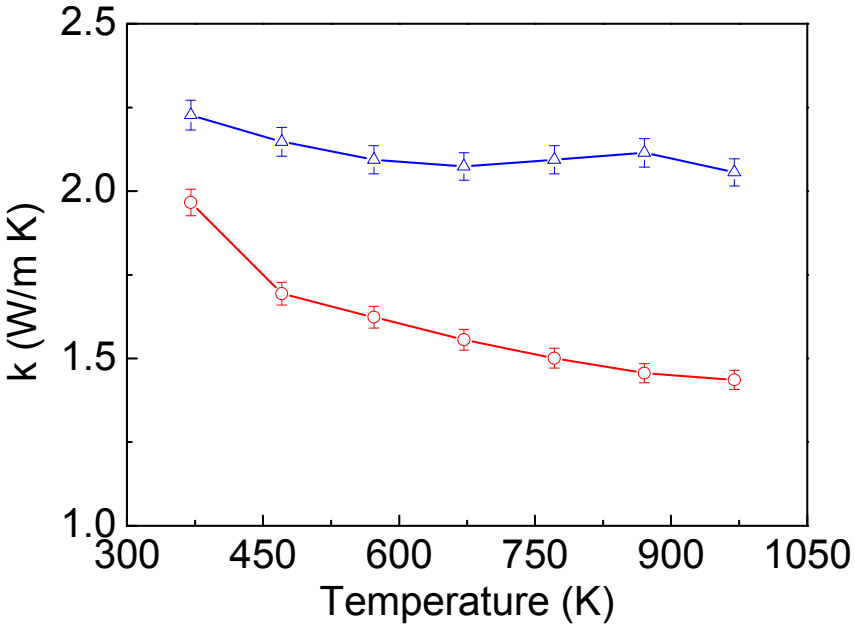

Figure 6 Temperature dependence of the thermal conductivity: (Circle) La-1, (Triangle) La-2/3

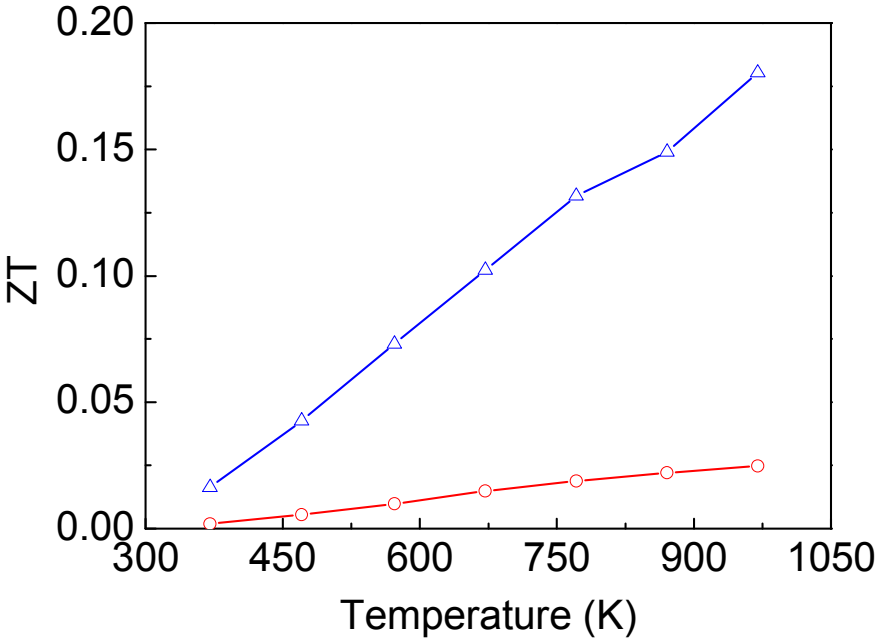

Figure 7 Temperature dependence of dimensionless figure of merit ZT: (Circle) La-1, (Triangle) La-2/3

Finally, the temperature dependence of dimensionless figures of merit for the La-2/3 and La-1 ceramic samples is shown in **Figure 7**. Despite the large thermal conductivity, the highest thermoelectric ZT was achieved by the La-2/3 sample with

0.18 at 973 K, which was almost one order of magnitude higher than that of the La-1 sample.

Conclusions

Lanthanum titanate ceramics with different La/Ti ratio were synthesized using sol-gel method followed by conventional sintering process. SEM image revealed that the as-prepared Lanthanum titanate ceramic has a relatively high density with an average grain size of 5 – 20 μm. By introducing La vacancy and providing oxygen defect in the crystal structure, pure phase of $La_{2/3}TiO_{2.87}$ ceramic was synthesized. For the first time, the thermoelectric properties of $La_{2/3}TiO_{2.87}$ ceramic have been investigated. The as-prepared $La_{2/3}TiO_{2.87}$ ceramic showed a large power factor with high electrical conductivity and enhanced Seebeck coefficient with low thermal conductivity over 373-973 K. The resultant dimensionless ZT value of 0.18 at 973K by the pristine La2/3TiO3 sample is comparable to the performance of other n-type oxide-based thermoelectric materials, such as $SrTiO_3$, In_2O_3 and $CaMnO_3$. This indicates that bulk $La_{2/3}TiO_{2.87}$ could become potential candidates for high-temperature applications. It is expected that the thermoelectric performance of $La_{2/3}TiO_{2.87}$ can be further enhanced by doping engineering or nano-engnineering.

Acknowledgement

The authors would like to acknowledge the financial support from the Australian Research Council Project of FT140100032.

Reference

1. D. M. Rowe, CRC/Taylor & Francis, Boca Raton, 2006.
2. T. Okuda, K. Nakanishi, S. Miyasaka and Y. Tokura, *Physical Review B*, 2001, **63**.
3. H. Muta, K. Kurosaki and S. Yamanaka, *Journal of Alloys and Compounds*, 2003, **350**, 292-295.
4. K. Koumoto, R. Funahashi, E. Guilmeau, Y. Miyazaki, A. Weidenkaff, Y. Wang, C. Wan and X. D. Zhou, *Journal of the American Ceramic Society*, 2013, **96**, 1-23.
5. M. Ohtaki, H. Koga, T. Tokunaga, K. Eguchi and H. Arai, *Journal of Solid State Chemistry*, 1995, **120**, 105-111.
6. K. Koumoto, Y. Wang, R. Zhang, A. Kosuga and R. Funahashi, *Annual Review of Materials Research*, 2010, **40**, 363-394.
7. P. A. Fuierer and R. E. Newnham, *Journal of the American Ceramic Society*, 1991, **74**, 2876-2881.
8. Y. Taguchi, T. Okuda, M. Ohashi, C. Murayama, N. Môri, Y. Iye and Y. Tokura, *Physical Review B*, 1999, **59**, 7917-7924.
9. M. Nistor and J. Perrière, *Solid State Communications*, 2013, **163**, 60-64.
10. I.-S. Kim, T. Nakamura, Y. Inaguma and M. Itoh, *Journal of Solid State Chemistry*, 1994, **113**, 281-288.
11. K. H. Kim, D. P. Norton, J. D. Budai, M. F. Chisholm, B. C. Sales, D. K. Christen and C. Cantoni, *physica status solidi (a)*, 2003, **200**, 346-351.
12. S. Gariglio, J. W. Seo, J. Fompeyrine, J. P. Locquet and J. M. Triscone, *Physical Review B*, 2001, **63**, 161103.
13. D. A. Muller, N. Nakagawa, A. Ohtomo, J. L. Grazul and H. Y. Hwang, *Nature*, 2004, **430**, 657-661.
14. S. D. Yoon, Y. Chen, A. Yang, T. L. Goodrich, X. Zuo, D. A. Arena, K. Ziemer, C. Vittoria and V. G. Harris, *Journal of Physics: Condensed Matter*, 2006, **18**, L355-L361.
15. S. Madhukar, S. Aggarwal, A. M. Dhote, R. Ramesh, A. Krishnan, D. Keeble and E. Poindexter, *Journal of Applied Physics*, 1997, **81**, 3543.
16. R. Kabir, T. Zhang, D. Wang, R. Donelson, R. Tian, T. T. Tan and S. Li, *Journal of Materials Science*, 2014, **49**, 7522-7528.
17. T. Kolodiazhnyi, A. Petric, M. Niewczas, C. Bridges, A. Safa-Sefat and J. Greedan, *Physical Review B*, 2003, **68**, 085205.
18. Z. P. Gao, H. X. Yan, H. P. Ning, R. Wilson, X. Y. Wei, B. Shi, H. Ye and M. J. Reece, *J.Euro.Ceram.Soc.*, 2013, **33**, 1001-1008.
19. M. Cutler and N. Mott, *Physical Review*, 1969, **181**, 1336-1340.
20. L. K. Joseph, Cochin University of Science and Technology, 2009.